Viscosity and density stratification in vertical Poiseuille flow

Yuriko Renardy

Citation: Physics of Fluids (1958-1988) **30**, 1638 (1987); doi: 10.1063/1.866228
View online: http://dx.doi.org/10.1063/1.866228
View Table of Contents: http://scitation.aip.org/content/aip/journal/pof1/30/6?ver=pdfcov
Published by the AIP Publishing

Viscosity and density stratification in vertical Poiseuille flow

Yuriko Renardy
Department of Mathematics, 460 McBryde Hall, Virginia Polytechnic Institute and State University, Blacksburg, Virginia 24061-4097

(Received 29 October 1986; accepted 16 March 1987)

The linear stability of plane three-layer vertical Poiseuille flow is considered. The layers are composed of two immiscible fluids, one next to the walls and one centrally located. The fluids have different viscosities and densities and surface tension effects are included. Intuitively, an analogy with the concentric Hagen–Poiseuille flow is expected and the similarities and differences are investigated. The ability of heuristic reasoning to predict which arrangements are more likely to be observed is tested. Numerical results concerning low Reynolds numbers, as well as the behavior of eigenvalues close to the first criticality of the one-fluid problem, are presented.

I. INTRODUCTION

We consider the linear stability of three-layer vertical Poiseuille flow in the presence of gravity. The layers next to the walls are assumed to be of the same thickness and to be the same fluid. The two fluids are immiscible, have different viscosities and densities, and there is surface tension at the interfaces. Intuitively, this may be expected to model vertical concentric pipe flow of two fluids in some sense. There is considerable interest in such a flow because of applications in industry[1–8] involving situations where the densities of the fluids are similar, as well as when they are not similar. The main problem in this area lies in providing satisfactory reasons as to why only certain arrangements are reportedly observed in experiments. The results of this paper indicate that those reasons are far from obvious.

In steady parallel shear flows that involve layers of immiscible fluids, there is the theoretical question of what arrangements are more likely to be observed than others. In theory, given the volumes occupied by the fluids, many arrangements are possible. On the other hand, experimental results document that certain arrangements are preferred. For example, Southern and Ballman[5] investigate the effect of viscosity stratification in pipe flow. They find that as the fluids travel through the pipe under pressure, the less viscous fluid tends to migrate to the pipe wall and encapsulate the more viscous fluid, so that finally a steady encapsulated flow occurs. A number of other works agree with this and attempt to provide reasons for the encapsulation. One such heuristic reasoning is based on the idea that fluids prefer to position themselves so as to do the least amount of work. Because this is a conjecture without a firm basis, this became known as the "viscous dissipation principle." The principle aided some workers in justifying why the encapsulation occurred and gained some popularity.

A mathematical formulation of the viscous dissipation principle for the case of viscosity stratification has been explored in Ref. 9 and the results indicate that the principle is not totally wrong. This statement needs elaboration. The formulation, based on a straightforward interpretation of the heuristic idea and with no other justification, led to the following variational problem.[9] Given the volume of each fluid, locate the fluids such that the amount of viscous dissipation (or work) is minimized for a given flow rate. Obviously, surface tension appears nowhere. The effect of surface tension has since been shown[10] to include the suppression of short wave instabilities. The mathematical formulation of the viscous dissipation principle, for the case of viscosity stratification in pipe flow, leads to the unique solution that the less viscous fluid should be at the wall.[9] This did not, however, confirm that the principle was correct because a linear stability analysis of the pipe flow revealed that stability depends on the volume ratio[9] whereas the principle pays no attention to that. A linearly stable arrangement is one in which there is not too much of the less viscous fluid at the wall. If the less viscous fluid is centrally located, the arrangement is unstable. Thus, apart from the condition on the volume ratio and accounting for surface tension, the viscous dissipation principle does not compare too badly with the linear stability analysis. Other viscous stratified flows have been examined in the light of this principle. One example is the two-layer Taylor flow[11] where two fluids lie concentrically between two cylinders with the outer cylinder at rest and the inner one rotating. The principle predicts that the less viscous fluid should be next to the inner cylinder. However, the arrangement with a thin layer of the less viscous fluid next to either cylinder is found to be linearly stable. Here again, the principle is not totally wrong.

For the three-layer plane Poiseuille flow considered in this paper, the principle predicts that the less viscous fluid should be located next to the walls in the case of pure viscosity stratification. Surprisingly, this is in total agreement with the results of Than, Rosso, and Joseph who considered the linear stability of the interface to long wave disturbances[12] and found no dependence of criticality on the volume ratio. However, since an instability need not arise necessarily from long waves, we extend the work of Ref. 12 to cover all wavelengths for the case of viscosity stratification. There are situations that are stable to long wave disturbances, and are not stable to order-1 wave disturbances. An example of such a situation is presented in Sec. IV.

So far, in stability analyses for multilayer flows, little attention has been paid to the question of the location of largest growth rates. We examine particular situations and find that in the absence of surface tension, the largest growth rates occur at order-1 wavenumbers and not in the long wave

 0031-9171/87/061638-11$01.90

or short wave ranges. Surface tension is effective in cutting down the growth rate and slightly shifts the wavenumber at which it peaks towards the longer waves.

In the case of density stratification, we mimic the heuristic idea that the fluids prefer to arrange themselves in order to flow with the least amount of work. Hence, we expect that the flow should place the heavier fluid at the center for downward flow and at the walls for upward flow. We show in Sec. IV that our numerical results on linear stability for long waves agree with the heuristic idea in some respects. Keeping in mind that the heuristic argument neglects effects such as surface tension and volume ratio, the amount of agreement attained is encouraging, but on the other hand, the amount of disagreement makes that idea only a guiding one in practice.

One reason why both pipe flow and plane flow may be expected to behave analogously is that the plane flow is intuitively equated to a cross section of the pipe flow. This analogy is expected to be a reasonable one when the fluid at the walls in both flows is in a sufficiently thin layer. Our results in Sec. IV bear this out. Namely, the arrangement with a thin layer of the less viscous fluid at the wall can be stable in both flows. In this connection, situations close to the first criticality of the corresponding one-fluid problem have been examined. The type of behavior that was found in two-layered Taylor flow[11] is also found here for the plane Poiseuille flow. That is, one might expect that the addition of a less viscous fluid to a one-fluid problem at criticality would promote the onset of instability. However, the addition of a thin layer of a less viscous fluid at the walls delays the onset of criticality. This phenomenon has been referred to in Ref. 12 as a "lubrication stabilization."

The equations governing the linear stability analysis are presented in Sec. II. We use normal mode analysis and assume that perturbations depend on time through the factor $\exp(\sigma t)$ and are periodic in the streamwise direction with wavenumber α. We solve for the complex-valued eigenvalues σ as a function of all the other parameters. There are two types of eigenvalues: those that are associated with (i.e., branch from) eigenvalues of the corresponding one-fluid problem, which are referred to in this paper as "one-fluid modes," and those that arise from the presence of the interfaces. When we restrict ourselves to low Reynolds numbers, the one-fluid eigenvalues are linearly stable and we only need to examine the interfacial eigenvalues for stability. It is known[13] that the interfacial eigenvalues can become unstable at any Reynolds number. We consider both low Reynolds numbers and higher Reynolds number around that of the first criticality of the one-fluid problem. The numerical method we use for computing the eigenvalues is a spectral method and is described in Sec. III. This method yields all the eigenvalues, not just the interfacial ones. In Sec. IV, numerical results are discussed.

II. FORMULATION OF EQUATIONS

We consider linear stability of three-layer Poiseuille flow as shown in Fig. 1. We use the following dimensionless variables:

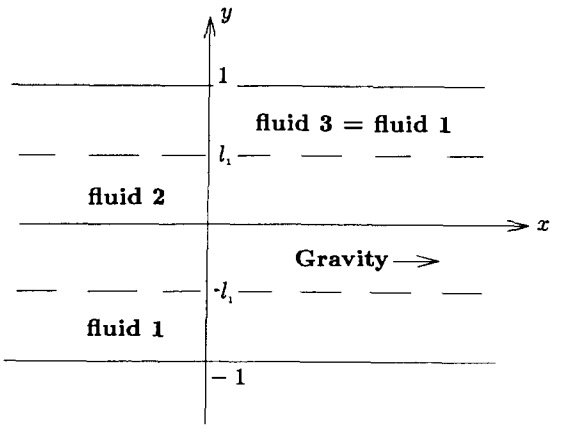

FIG. 1. Undisturbed three-layer Poiseuille flow.

$$(x,y) = (x^*,y^*)/l^*, \quad (u,v) = (u^*,v^*)/\sqrt{gl^*},$$
$$p = p^*/\rho_1 g l^*, \quad t = t^*\sqrt{g/l^*},$$

where the asterisks denote dimensional quantities, l^* denotes half the plate separation, ρ_1 denotes the density of fluid 1, and g denotes gravitational acceleration acting in the x direction. We prescribe a pressure gradient $\partial P^*/\partial x^* = G^*$, which, in dimensionless form, is $\partial P/\partial x = G^*/\rho_1 g$, where P is the undisturbed pressure. The undisturbed flow is symmetric about the x axis and consists of flat interfaces at $y = \pm l_1$, fluid 1 occupies $-1 \leqslant y \leqslant -l_1$ and $l_1 \leqslant y \leqslant 1$, and fluid 2 occupies $-l_1 \leqslant y \leqslant l_1$. Fluid i has density ρ_i, viscosity μ_i, and kinematic viscosity ν_i. S^* denotes the dimensional surface tension coefficient. There are six dimensionless parameters: l_1, m, r, R_1, G, and S defined by

$$m = \mu_1/\mu_2, \quad r = \rho_1/\rho_2,$$
$$R_i = l^*\sqrt{gl^*}/\nu_i, \quad G = G^*/\rho_1 g, \quad S = S^*/\rho_1 g l^*.$$

We refer to R_1 as a reference Reynolds number. The undisturbed velocity is $[U(y),0]$, which satisfies the no slip conditions at $y = \pm 1$. At the interfaces $y = \pm l_1$, it satisfies the continuity of velocity

$$[\![U]\!] = 0, \tag{1}$$

where $[\![x]\!]$ denotes $x_1 - x_2$, and continuity of shear stress

$$\left[\!\!\left[\mu \frac{\partial U}{\partial y}\right]\!\!\right] = 0, \tag{2}$$

and the normal stress condition is satisfied by the flat interfaces and the jump in the basic pressure being zero. We note that the shear stress at the interfaces vanishes when $Gr = 1$. Hence,

$$\begin{aligned} U(y) &= R_1(G-1)y^2/2 + c_1 y + c_2, \quad -1 \leqslant y \leqslant l_1, \\ &= R_2(Gr-1)y^2/2 + c_3, \quad -l_1 \leqslant y \leqslant l_1, \\ &= R_1(G-1)y^2/2 - c_1 y + c_2, \quad l_1 \leqslant y \leqslant 1, \end{aligned} \tag{3}$$

$$c_1 = R_1 l_1 (1/r - 1), \quad c_2 = R_1[l_1(1/r-1) - 0.5(G-1)],$$

$$c_3 = R_1\left[(G-1)\left(\frac{-l_1^2}{2} + l_1 - 0.5\right) + \frac{m}{r}(Gr-1)\left(\frac{-l_1^2}{2} + \frac{l_1^2}{m} - \frac{l_1}{m}\right)\right].$$

The perturbed velocity is

$$U(y)\underline{i} + \epsilon[u(y),v(y)]\exp(i\alpha x + \sigma t),$$

the pressure is $P + \epsilon p(y)\exp(i\alpha x + \sigma t)$, and the interfaces are at $y = -l_1 + \epsilon h_1 \exp(i\alpha x + \sigma t)$, $y = l_1 + \epsilon h_2 \times \exp(i\alpha x + \sigma t)$, where ϵ is small. The equations for a small disturbance are

$$[\sigma + i\alpha U(y)]\Delta v - i\alpha v U_{yy}(y) = (1/R_i)\Delta^2 v, \tag{4}$$

where

$$\Delta = \frac{\partial^2}{\partial y^2} - \alpha^2,$$

and

$$i\alpha u + v_y = 0. \tag{5}$$

At the interfaces, the kinematic condition yields

$$v = h_i(\sigma + i\alpha U); \tag{6}$$

the velocity is continuous,

$$[\![h_i U_y + u]\!] = 0, \tag{7}$$

$$[\![v]\!] = 0; \tag{8}$$

the shear stress is continuous,

$$[\![\mu(U_{yy}h_i + u_y + i\alpha v)]\!] = 0; \tag{9}$$

and the normal stress balance yields

$$\left[\!\!\left[-p + 2\frac{\mu}{\mu_1 R_1}\frac{\partial v}{\partial y}\right]\!\!\right] = -S\alpha^2 h_1 \quad \text{at } y = -l_1$$
$$= S\alpha^2 h_2 \quad \text{at } y = l_1, \tag{10}$$

where

$$(\rho_1/\rho_i)i\alpha p = (1/R_i)\Delta u - \sigma u - i\alpha u U - v U_y.$$

When the two fluids have identical properties, and surface tension is zero, Eqs. (4)–(10) are satisfied by the following velocity and interfacial disturbances, which is called the "interfacial mode":

$$u = v = 0, \quad \sigma = -i\alpha U(l_1), \quad h_1 = h_2 = 1. \tag{11}$$

III. NUMERICAL METHOD

For numerical computations, the variables u and p are eliminated and the Chebyshev-tau method[14,15] is used to discretize the variable $v(y)$. This method approximates discrete eigenvalues of C^∞ eigenfunctions with infinite-order accuracy.

The variable v is expanded in a series of Chebyshev polynomials[14] $T_n(z)$, defined by $T_n(\cos\theta) = \cos n\theta$ when $z = \cos\theta$, and truncated. A feature of the tau method is that the expansion polynomials are not required individually to satisfy the boundary conditions. Rather, the boundary conditions are imposed as part of the conditions determining the eigenvalues. We map the y interval for each fluid onto the interval $[-1,1]$ on which the Chebyshev polynomials live, and note that the Chebyshev polynomial of even degree is symmetric and that of odd degree is antisymmetric.

We construct the computer program to handle a three-layer problem with three different fluids for reasons explained below. If N is the highest degree of the Chebyshev polynomials used to represent v, then they contribute $N+1$ unknowns in each fluid. Including the unknowns h_1 and h_2, there are $3N+5$ unknowns. Equation (4) is represented correctly up to degree $N-4$ so that the number of equations is $3(N-3)$ plus five conditions at each interface and four boundary conditions. The eigenvalues of the $3N+5$ matrix are computed in quadruple precision on a VAX 11/785 computer. Since the problem is symmetric in the vertical variable y, the two interfacial eigenfunctions are composed of one symmetric in y and an antisymmetric one. Since we can also calculate the coefficient vector for each eigenfunction, we can find out which eigenvalue belongs to the symmetric mode and which to the antisymmetric. The coefficient vector is of the form (v_1,v_2,v_3,h_1,h_2), where v_i represents the coefficients of the Chebyshev polynomials up to degree N for the component of the perturbation velocity in the y direction in fluid i and fluid 3 is defined in the next paragraph to be the uppermost fluid. If the mode is symmetric, entries for v_2 are nontrivial for the coefficients of the Chebyshev polynomials of even degree. If the mode is antisymmetric, the entries for odd degree polynomials for v_2 are nontrivial. If a mode is antisymmetric, then by the continuity equation, the component of velocity in the x direction is symmetric so that the mode will be referred to as "varicose." Similarly, a mode symmetric in v will be referred to as "snake." The shape of the interface for these modes are illustrated in Ref. 12.

The computer program for the calculation of σ was constructed for a genuine three-layer problem with three different fluids, fluid 3 in undisturbed flow occupying $l_3 < y < 1$, and with the undisturbed interfaces at $y = -l_1$ and $y = l_3$. The reason for doing this is that by letting two adjacent layers be the same fluid, the interfacial eigenvalues could be checked against the long wave asymptotics for two-layer Poiseuille flow of Yih.[13] The interfacial eigenvalue was checked with Yih's Fig. 3 at his values of $m = 2$ and $m = 30$ together with his equations (46) and (51). This checks both the real and imaginary parts of the eigenvalue. The eigenfunction for the two-layer Couette–Poiseuille flow of Yih is a seventh degree polynomial in y at this order of α, just as in the case of long waves for our three-layer problem. In our three-fluid computer program, when fluids 1 and 2 have identical properties, a further consistency check is that one interfacial eigenvalue is neutrally stable while the other must be independent of l_1. A similar consistency check was made when fluids 2 and 3 have identical properties. The program was checked against the one-fluid result for criticality,[16] and against the short wave asymptotics for viscosity stratification,[10] namely,

$$\sigma \sim -i\alpha U(l_1) + \frac{R_1^3 l_1^2 (m-1)m^2}{\alpha^2 2(m+1)^2 r^2}$$
$$\times (Gr-1)^2\left(\frac{-1}{m} + \frac{m}{r}\right) - \frac{\alpha R_1 Sm}{2(m+1)},$$

for large α and $S\alpha^3 = O(1)$. All numerical results presented in this paper have been tested for convergence.

We note that the equations in Li's paper[17] contain results for the long wave approximation to the interfacial eigenvalues for our flow implicitly and it should be possible to extract the results by letting his parameter A, representing the pressure gradient, be large compared with 1 (which is

essentially the scale of the speed of his top plate) in his equations. This is easily done for the oscillatory part of the eigenvalue. Unfortunately, he does not explicitly define some of his notation, for example, in his Sec. 4B, so that one would have to repeat his calculations to retrieve the growth rates. The long wave analysis of Than, Rosso, and Joseph[12] was checked against our computed results.

We remark in passing that the algebra required in analyzing the long wave asymptotics[12,17] is long and in order to find out the neutral stability curves or the growth rates from the resulting closed form expressions, numerical computations are usually *ultimately* required. The energy expended for this may be as much if not more than the energy expended in writing a computer program for the original problem without the long wave approximation. It is evident that the two types of works need to be done simultaneously, not only to complement each other (which is important) but to check each other.

IV. RESULTS AND DISCUSSION

A. Viscosity stratification

We consider low Reynolds numbers. We begin with some results on long waves. Figures 2–4 exhibit the growth rates for long wave disturbances of the two interfacial eigenvalues for the case of equal density. Their growth rates are proportional to α^2 and $\mathrm{Im}(\sigma)$ is proportional to α as α tends to 0. All other eigenvalues of the problem are linearly stable at this Reynolds number. Surface tension is chosen to be zero because Eq. (10) shows that the effect of surface tension for small α is negligible. The case of equal viscosity is a critical one: if the outer fluid is the more viscous, both eigenvalues are unstable and otherwise, both are linearly stable. In this respect, there appears to be qualitative agreement with the long wave analysis of Li for three-layer Couette flow.[17] Although it is not possible to immediately evaluate the neutral stability curves from his paper, he did present numerical results for specific sets of parameter values. Li's Figs. 4(a), 4(b), and 5(a)–5(c) for the case of his $m_b = m_a$ (the fluids next to the walls have the same viscosity) display computed results that indicate that if the less viscous fluid is central, the flow is unstable and otherwise it is linearly stable. On the other hand, the lack of dependence of criticality on the volume ratio is unexpected from past results on other two-layer flows.[11,18–20] In the concentric two-layer pipe flow, linear stability has displayed a "thin-layer effect" for long waves, i.e., if the less viscous fluid lies in a thin layer next to the pipe wall, the arrangement tends to be stable whereas if there is too much of the less viscous fluid, the arrangement is unstable. Our results on the plane flow do not contradict the thin-layer effect. However, the instability of a thick layer of the less viscous fluid is absent. Hence, when the fluid at the walls is in thin layers, there is qualitative similarity between the pipe and plane flows. We see below that criticality will depend on the volume ratio for larger wavenumbers or larger Reynolds numbers and the instability of a thick layer of less viscous fluid described above returns for such parameters.

It is of interest to find out what wavenumbers display the largest growth rates: Do they occur at long waves, short waves, or in the middle? Which wavelengths are the most dangerous? In the case of instability, how significant is the long wave instability compared with other wavelengths? These questions have not been previously investigated for layered shearing flows. We have examined two situations: one where there is long wave instability and one where long waves are stable. We chose a value of l_1 where the long wave instability has relatively large growth rates. Based on Figs. 2–4, we chose $l_1 = 0.5$. We choose the reference Reynolds number R_1 to be 1.0 and choose the pressure gradient parameter to be $G = 3.0$. Our parameters are $m = 2$ for the case of long wave instability (Fig. 5) and $m = 0.5$ for the case of long wave stability (Fig. 6). In Fig. 5, the growth rates for $S = 0$ and 0.001 are pictorially the same until α is about 2. In Fig. 6, they are similar until α reaches about 2.5. In both

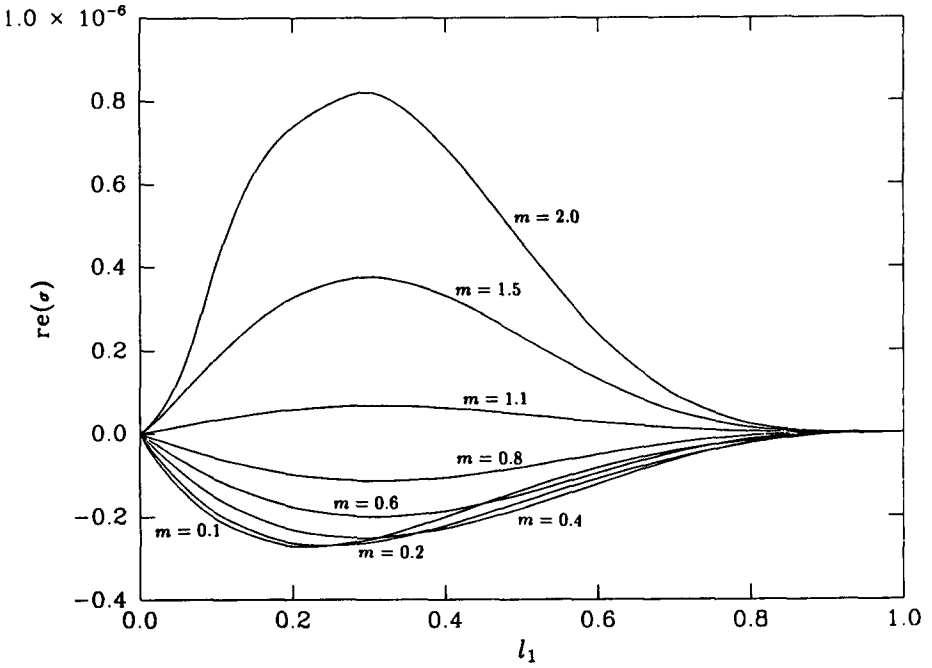

FIG. 2. The growth rate $re(\sigma)$ of the interfacial snake mode versus l_1 for long waves. $R_1 = 1.0$, $G = 3.0$, $\alpha = 0.01$, zero surface tension, no density difference.

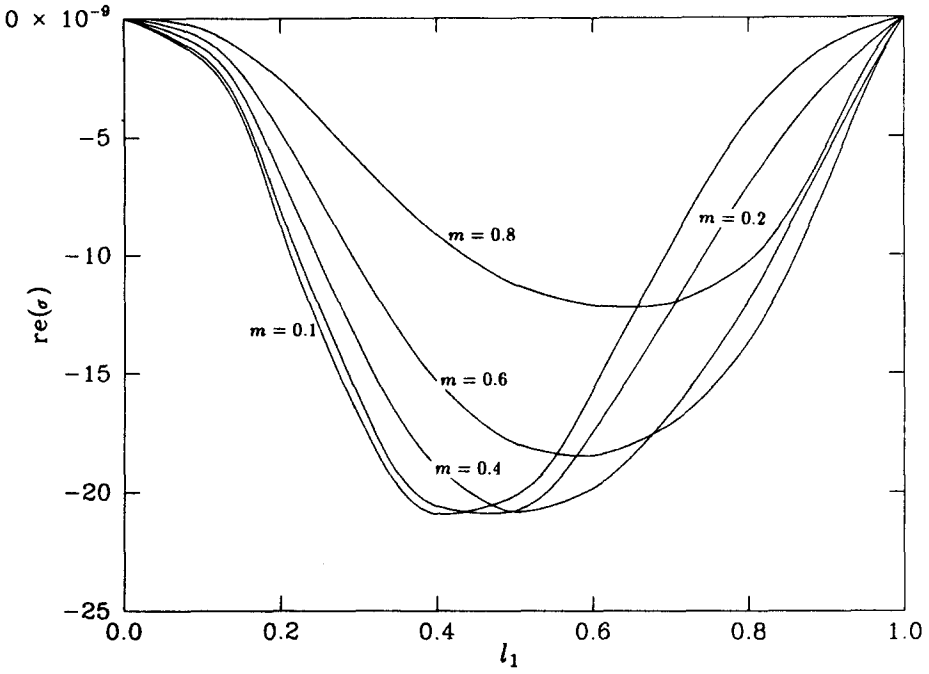

FIG. 3. The growth rate $re(\sigma)$ of the interfacial varicose mode versus l_1 for long waves. $R_1 = 1.0$, $G = 3.0$, $\alpha = 0.01$, zero surface tension, no density difference, $m < 1.0$.

figures, the growth rates for $S = 0$ and 0.01 are similar until α reaches about 1. In both cases, if surface tension is zero, the growth rates reach peaks of similar magnitude at order-1 wavenumbers. The peaks do not lie in the long wave or short wave range, thus emphasizing the importance of examining what happens at order-1 wavelengths. The effect of surface tension in killing the short wave instabilities is also illustrated. The figures show that surface tension is effective in suppressing the peak and slightly shifts it to longer waves. The long wave analysis of Than, Rosso, and Joseph[12] yields an uncomplicated criterion for instability. It is evident that the criterion is more complicated for waves that are not long, for which the volume ratio and surface tension enter in a significant way and at which the largest growth rates often occur.

B. Density stratification: Long wave results

Intuition suggests that the fluids should arrange themselves in order to flow most easily, that is, to maximize the flow rate for a given pressure gradient. This leads one to expect that the heavier fluid should tend to stay at the center of the pipe for downward flow (to the positive x direction) and to stay at the walls for upward flow (to the negative x direction).

For long waves, a rough picture is that if the density difference is small, one mode is stable while the other is unstable, resulting in instability no matter which fluid is where. This is counter to our heuristic idea. This simple picture becomes complicated if the densities are not close. Unlike

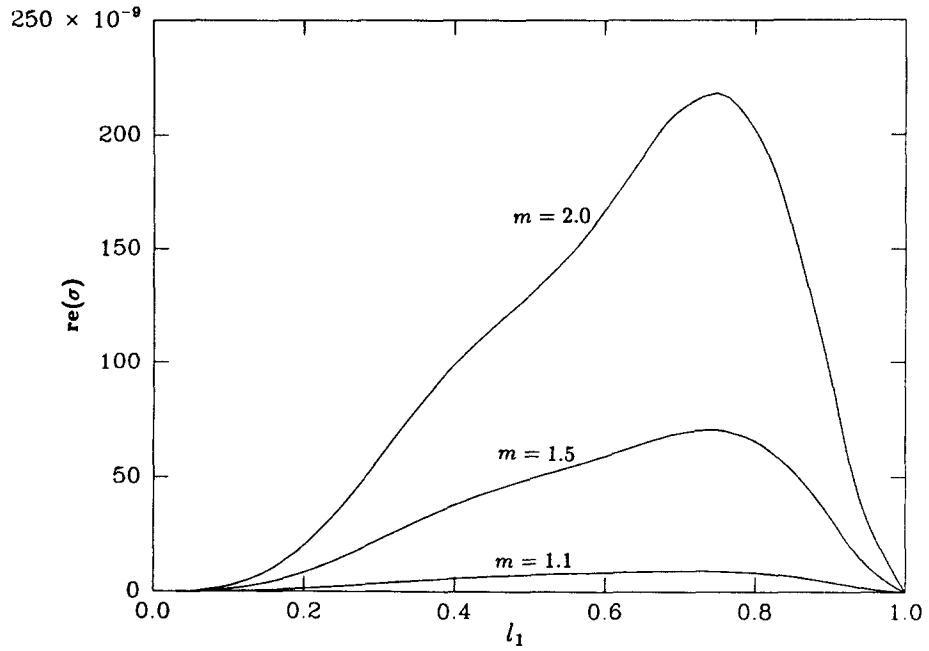

FIG. 4. The growth rate $re(\sigma)$ of the varicose mode versus l_1 for long waves. $R_1 = 1.0$, $G = 3.0$, $\alpha = 0.01$, zero surface tension, no density difference, $m > 1.0$.

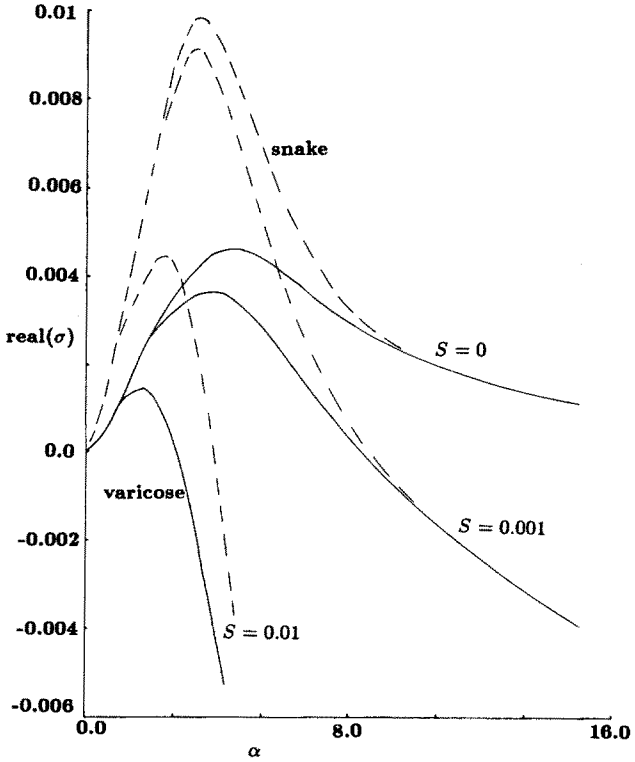

FIG. 5. The growth rates of both interfacial eigenvalues versus α for $R_1 = 1.0$, $G = 3$, $r = 1$, $m = 2$, $S = 0$, 0.001, 0.01, $l_1 = 0.5$. The full lines represent varicose modes and dashed lines are snake modes. For each value of surface tension, the snake and varicose modes coincide for large enough α.

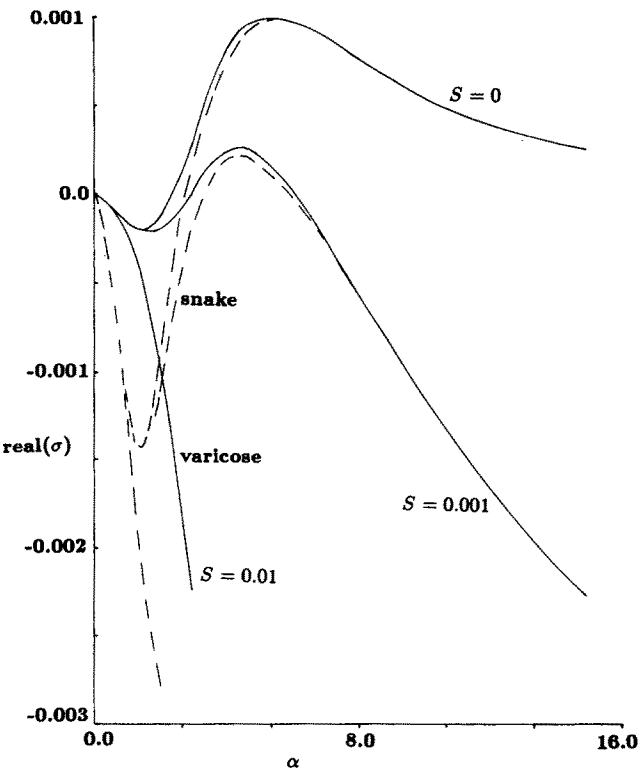

FIG. 6. The growth rates of both interfacial eigenvalues versus α for $R_1 = 1.0$, $G = 3$, $r = 1$, $m = 0.5$, $S = 0$, 0.001, 0.01, $l_1 = 0.5$. The full lines represent varicose modes and dashed lines are snake modes. For each value of surface tension, the snake and varicose modes coincide for large enough α.

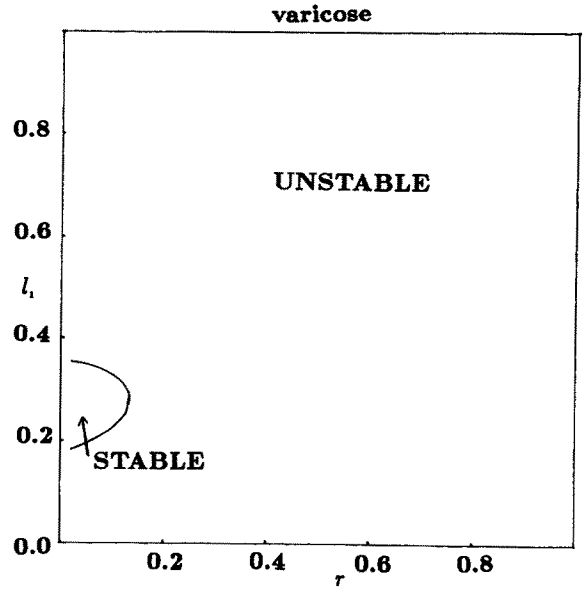

FIG. 7. Neutral stability curves for the varicose mode, $G = 0$, $R_1 = 1.0$, $\alpha = 0.01$, surface tension = 0, $0.02 \leqslant r \leqslant 1$, $m = 1$, $0 \leqslant l_1 \leqslant 1$.

the long wave results for viscosity stratification, long wave results for density stratification depend on the volume ratio. We find regions (somewhat like "islands" in parameter space) where stability changes. When the densities are markedly different, our results are not totally in disagreement with heuristics. Details are given in the following paragraphs.

For flows in the direction of gravity (to the positive x direction), computations were performed at $G = 0$, $m = 1$, $R_1 = 1$, $\alpha = 0.01$, $S = 0$, and r between 0.05 and 10.0. These are downward flows. Figure 7 displays the neutral stability curves for $r \leqslant 1$, i.e., when the heavier fluid is central, for the varicose mode. Figure 8 displays the neutral stability curve for the snake mode. When r is slightly less than 1, a varicose instability occurs. However, the growth rate of the varicose

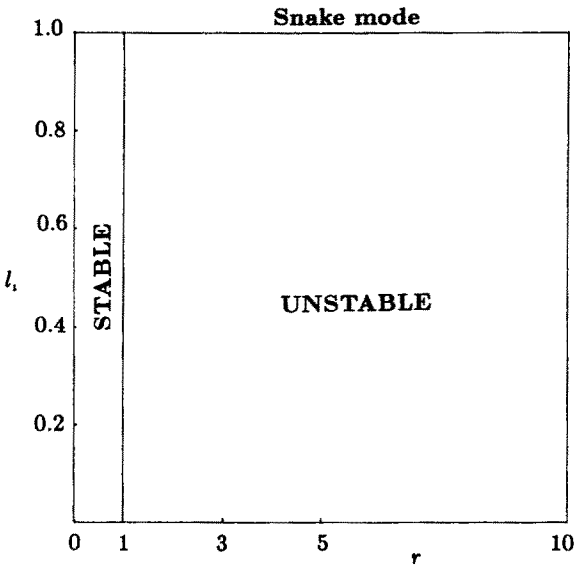

FIG. 8. Neutral stability curves for the snake mode, $G = 0$, $R_1 = 1.0$, $\alpha = 0.01$, surface tension = 0, $0 \leqslant r \leqslant 10$, $m = 1$, $0 \leqslant l_1 \leqslant 1$.

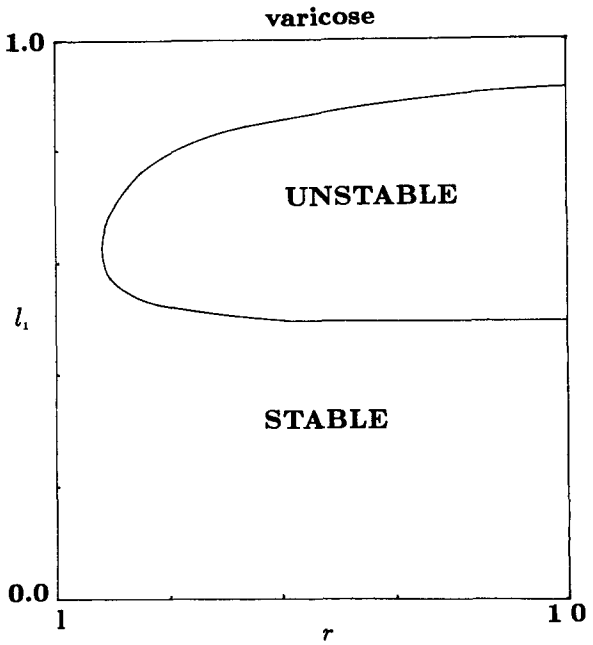

FIG. 9. Neutral stability curves for the varicose mode, $G = 0$, $R_1 = 1.0$, $\alpha = 0.01$, surface tension $= 0$, $1 \leqslant r \leqslant 10$, $m = 1$, $0 \leqslant l_1 \leqslant 1$.

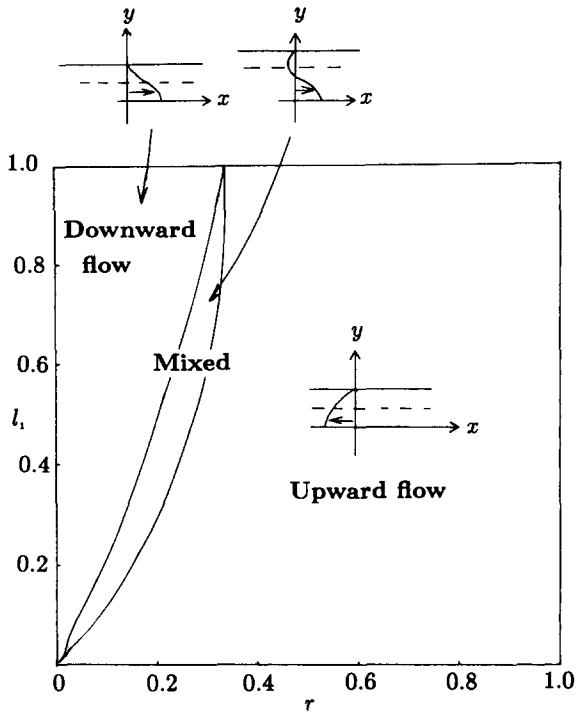

FIG. 10. Basic flows for $G = 3$, $R_1 = 1.0$, $m = 1$, $0.05 \leqslant r \leqslant 1$, $0 \leqslant l_1 \leqslant 1$.

mode begins to dip around $l_1 = 0.3$ as r decreases, until it actually becomes negative around $r = 0.14$. Thus there is an island of stability around $l_1 = 0.3$, as shown in Fig. 7. This is reminiscent of the island of stability in the graph of the neutral stability curve for odd disturbances in Ref. 12.

Figure 9 displays neutral stability curves for $r \geqslant 1$, i.e., when the outer fluid is heavier, for the varicose mode. We refer to Fig. 8 for the snake mode. Here, the snake mode is unstable. If r is not far from 1, the varicose mode is stable. However, as r increases away from 1, the varicose mode becomes unstable for the middle to upper range of l_1. In conclusion, for downward flow, long wave stability for our range of parameters occurs for $r \ll 1$ and l_1 around 0.3.

For flows forced in the direction against gravity, computations were performed at $G = 3.0$, $R_1 = 1$, $\alpha = 0.01$, $m = 1, S = 0$, and $0.05 \leqslant r \leqslant 10.0$. Figure 10 shows the variety of basic flows encountered here for $r < 1$. Not all of these flows are in the upward direction. Some flows involve backflow in the middle of the channel and a number of flows are in the downward direction. For $r \geqslant 1$, the basic flows are upward.

Parts of Figs. 11 and 12 display growth rates when the density difference is small. There is symmetry in $(r - 1)$ for r close to 1 as expected from a Taylor expansion about that

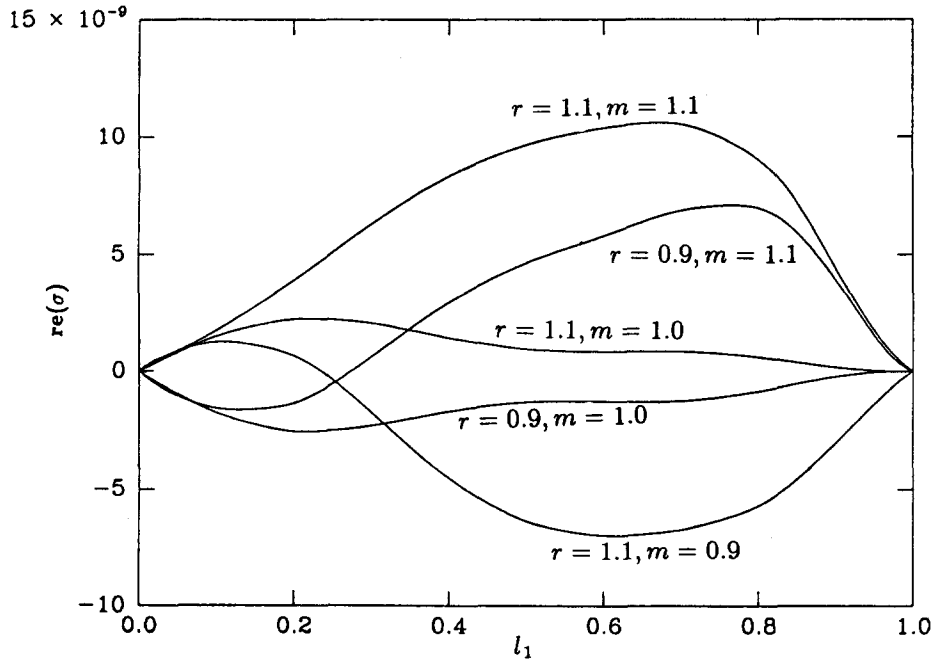

FIG. 11. The growth rate $re(\sigma)$ of the varicose mode versus l_1 for long waves. $R_1 = 1.0$, $G = 3.0$, $\alpha = 0.01$, zero surface tension, $r = 0.9$, 1.0, 1.1, and $m = 0.9$, 1.0, 1.1.

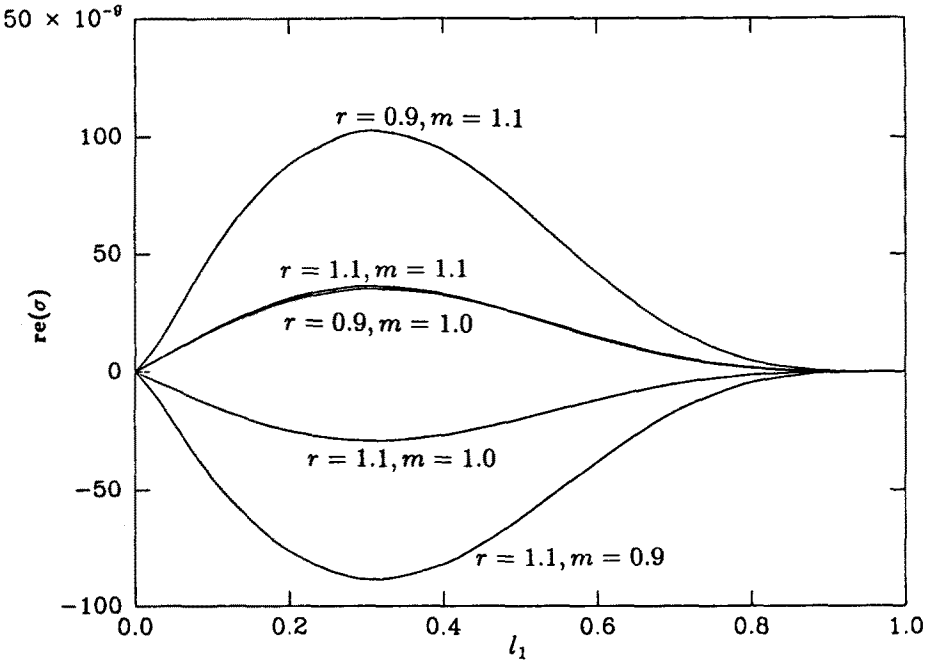

FIG. 12. The growth rate $re(\sigma)$ of the snake mode versus l_1 for long waves. $R_1 = 1.0$, $G = 3.0$, $\alpha = 0.01$, zero surface tension, $r = 0.9$, 1.0, 1.1, and $m = 0.9$, 1.0, 1.1.

value, just as there is symmetry in $(m - 1)$ for m close to 1 in Figs. 2–4. The roles of the modes are reversed from the case of downward flow. When the outer fluid is slightly heavier, the varicose mode is unstable. When the central fluid is slightly heavier, a snake instability occurs.

Figure 13 displays the neutral stability curve for the snake mode for $0.05 \leqslant r \leqslant 1$. The neutral stability curve coincides with the boundary in Fig. 10 where the basic flow changes from downward flow to a mixed flow with backflow in the middle of the channel. It appears that the stable region for the snake mode found in Fig. 13 actually reflects the stability of that mode for downward flow when r is less than 1. Therefore, for upward flow, the snake mode appears to be unstable for r less than 1.

Figure 14 displays the neutral stability curve for the varicose mode for $0.05 \leqslant r \leqslant 1$. The unstable region includes basic flows which are upward, downward and mixed. The stable region juts into the unstable region around $l_1 = 0.3$ for r less than 0.2, and there is linear stability of both the snake and varicose modes for an isolated island in the parameter space. However, the basic flows there are downward flows and the linear stability merely reflects the results discussed under the case $G = 0$.

Figures 15 and 16 display the neutral stability curves for the snake and varicose modes respectively, for $r \geqslant 1$, i.e., the outer fluid is heavier. Here, the snake mode is stable. The varicose mode is unstable when r is slightly greater than 1 but develops an island of stability around the middle to upper values of l_1 when r is large compared with 1. This behavior of the varicose mode is the reverse of the behavior for

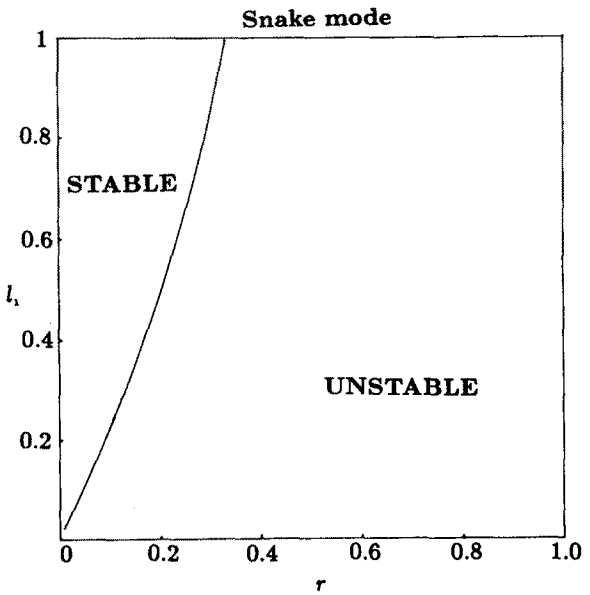

FIG. 13. Neutral stability curves for the snake mode, $0.05 \leqslant r \leqslant 1$, $R_1 = 1.0$, $G = 3.0$, $\alpha = 0.01$, zero surface tension, and $m = 1$.

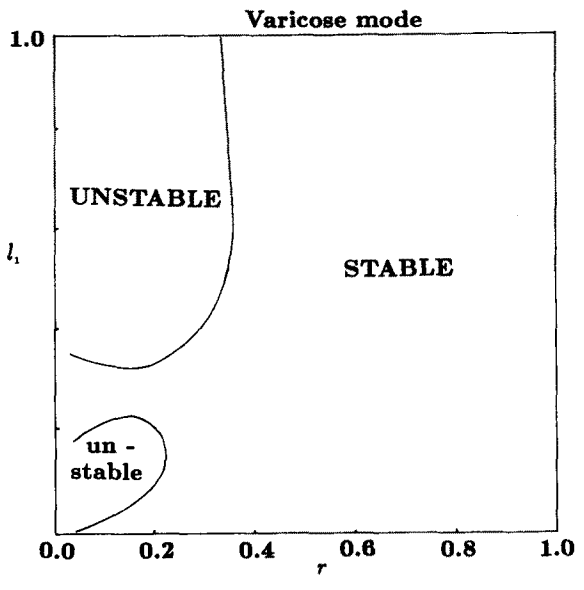

FIG. 14. Neutral stability curves for the varicose mode, $0.05 \leqslant r \leqslant 1$, $R_1 = 1.0$, $G = 3.0$, $\alpha = 0.01$, zero surface tension, and $m = 1$.

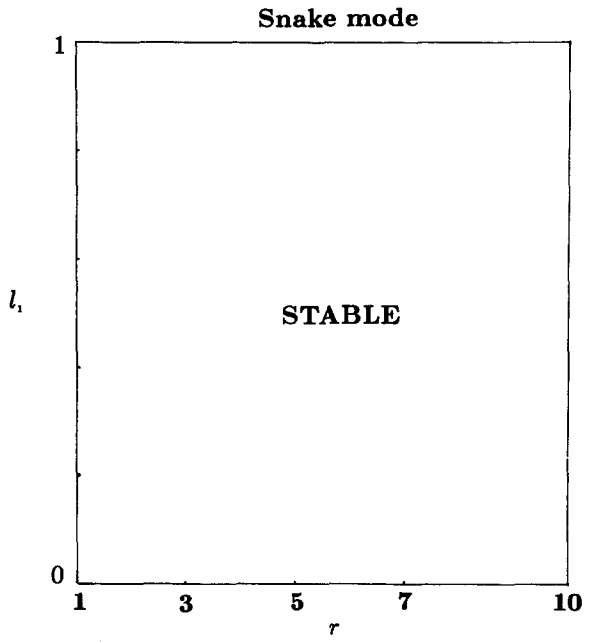

FIG. 15. Neutral stability curves for the snake mode, $1 \leqslant r \leqslant 10$, $R_1 = 1.0$, $G = 3.0$, $\alpha = 0.01$, zero surface tension, and $m = 1$.

downward flow when $r > 1$. For upward flow, we conclude that long wave stability for our range of parameters occurs for $r \gg 1$ in the island of stability as shown in Fig. 16. Based on our computations, long wave stability therefore occurs only for restricted values of the volume ratio and only for large density differences. In those cases, however, the arrangements of the fluids agree with the heuristic argument.

The effects of both viscosity and density stratifications are touched on next. For upward flow, Figs. 11 and 12 show the addition of density stratification on the data of Figs. 2–4. These do not involve large viscosity or density differences,

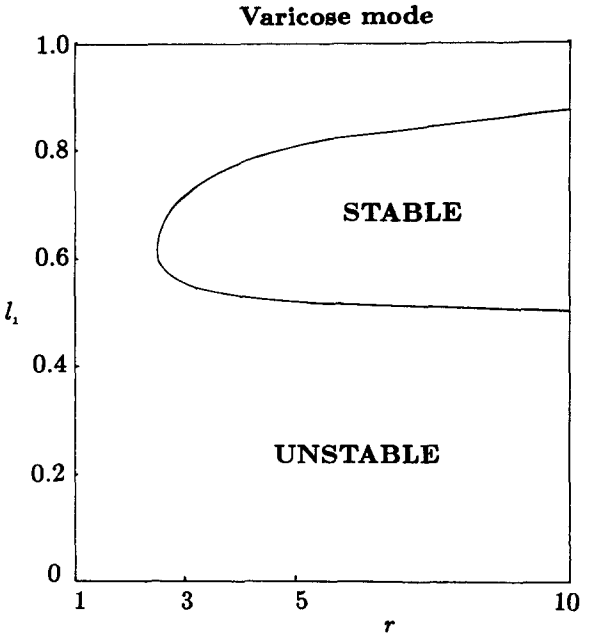

FIG. 16. Neutral stability curves for the varicose mode, $1 \leqslant r \leqslant 10$, $R_1 = 1.0$, $G = 3.0$, $\alpha = 0.01$, zero surface tension, and $m = 1$.

but show that their effects are additive and of similar magnitudes, confirming that they are competitive effects. If the central fluid is heavier, letting the fluid next to the walls be more viscous destabilizes the varicose mode causing both modes to be unstable for a wide range of volume ratios. If the fluid next to the walls is heavier, then putting the thin fluid at the center destabilizes the snake mode and both modes are unstable. Conversely, the instabilities caused by slight density stratification can be stabilized by putting the less viscous fluid at the walls.

The following is a summary of results for the case of low Reynolds numbers, suppressing details and all references to previous works.

(1) Three-layer Poiseuille flow (TLPF) with equal density may be linearly stable only if the more viscous fluid is centrally located. This stability occurs if the lubricating layer is relatively thin. Thick layers can be unstable to order-1 or short wave disturbances.

(2) TLPF with equal viscosity, falling under gravity, may be linearly stable only if the central fluid is markedly heavier. This stability occurs for a narrow interval of volume ratios.

(3) TLPF with equal viscosity, forced to flow against gravity, may be linearly stable only if the heavier fluid is outside. This stability occurs for a restricted range of volume ratios and when the densities are not similar.

C. Situations close to first criticality of the one-fluid flow

The first criticality of one-fluid plane Poiseuille flow occurs at approximately $\alpha = 1.020\,56$, $R_1 = 107.445\,06$,

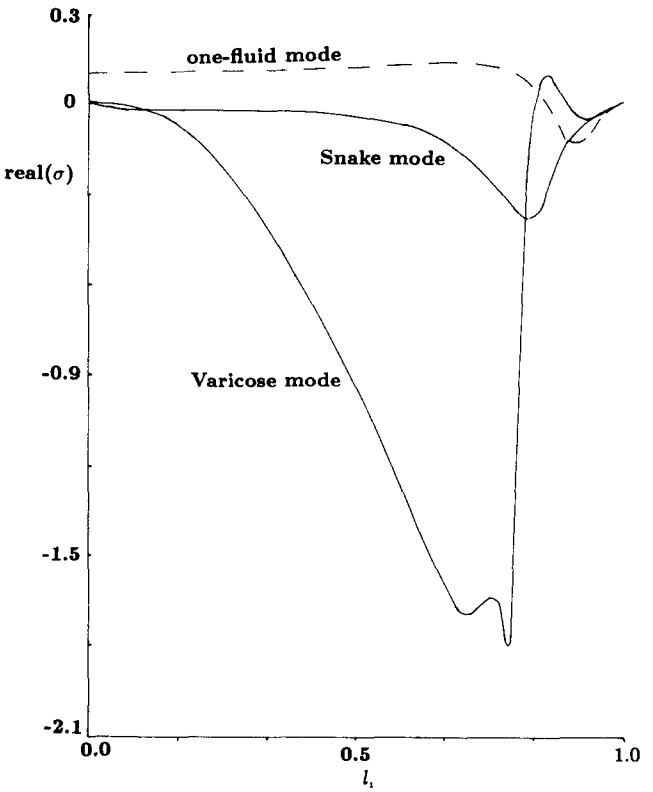

FIG. 17. The growth rates of the interfacial modes and the least stable one-fluid mode. $R_1 = 119.3834$, $\alpha = 1.020\,56$, $G = 0.0$, $m = 0.9$, zero surface tension, no density difference. The dashed line represents the least stable one-fluid mode.

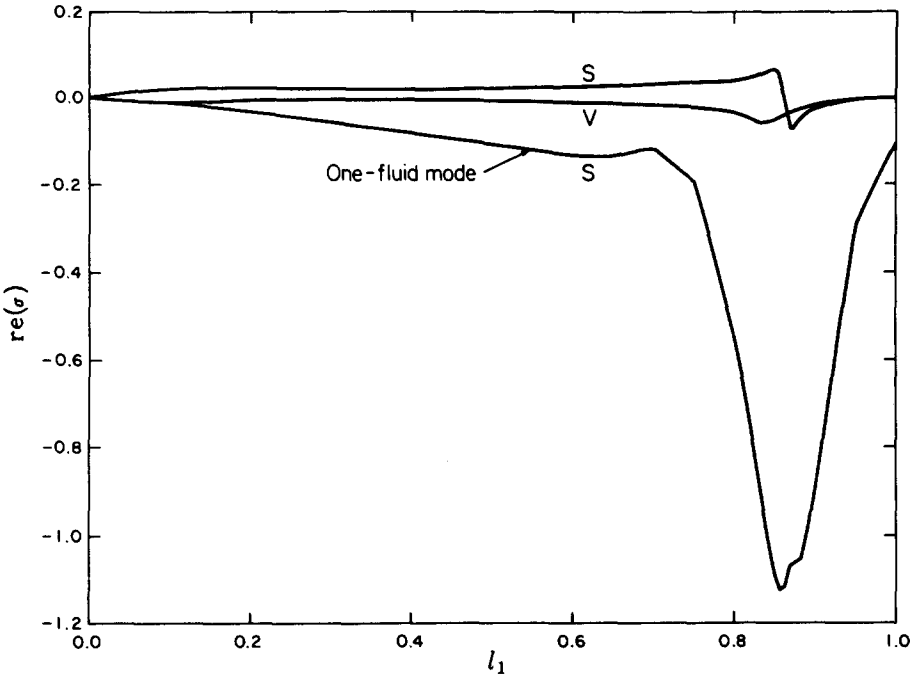

FIG. 18. The growth rates of the interfacial modes and the least stable one-fluid mode. $R_1 = 107.445\,06$, $r = 1.1$, $\alpha = 1.020\,56$, $G = 0.0$, zero surface tension, no viscosity difference. In the graph, S denotes the snake mode and V denotes the varicose mode. The least stable one-fluid mode is a snake mode.

$G = 0$, $S = 0$, and $m = r = 1$, in agreement with Refs. 15 and 16. Our reference Reynolds number R_1 is related to the Reynolds number Re of Drazin and Reid[16] through $\mathrm{Re} = R_1^2(1 - G)/2$. We examine the effects of viscosity and density stratification at this criticality for downward flow. Here, we examine the growth rates from the three eigenvalues. The marginally stable one-fluid eigenvalue has an even streamfunction; i.e., it is a snake mode (see Chap. 28, Ref. 16).

We first look at viscosity stratification. Figure 17 displays the growth rate for $R_1 = 119.3834$, $\alpha = 1.020\,56$, $m = 0.9$, and $r = 1.0$. Here, the central fluid is the more viscous and would be at criticality (that is, $R_2 = 107.445\,06$) if it filled the whole flow ($l_1 = 1.0$). The outer fluid would be above criticality if it were to occupy the entire flow ($l_1 = 0$). One may expect instability if a less viscous fluid is added to a flow at criticality. However, the curves close to $l_1 = 1$ show that the addition of a relatively thin layer of a less viscous fluid at the walls stabilizes the flow. As the amount of the less viscous fluid is increased ($l_1 = 0$ to about 0.89) instability occurs. This stabilizing effect of viscosity stratification when one of the fluids is in thin layers has been noted as a "lubrication" stabilization in two-layer Taylor flow.[11] At about $l_1 = 0.94$, the one-fluid mode, which is a snake mode, and the interfacial snake mode exchange identities. The graph at the junction around $l_1 = 0.9$ is reminiscent of the square-root function shape found in Figs. 9–12 of Ref. 11 where two branches merge into one. Here, the junction is not quite that shape because the parameters are not exactly at those of the crossover.

Figure 18 illustrates the effect of a small density difference on downward flow. The central fluid is lighter ($r = 1.1$) and would be below criticality if it were to occupy the entire flow, that is, if $l_1 = 1.0$. The outer fluid is at criticality if it occupies the entire flow, that is, if $l_1 = 0$. As the volume ratio varies from $l_1 = 0$ to 1, the least stable one-fluid mode and the varicose mode are linearly stable while the snake mode immediately becomes unstable and then stabilizes at about $l_1 = 0.863$. We remark that this dependence on the volume ratio is absent at low Reynolds numbers, as discussed in Sec. IV B. for the snake mode in downward flow for $r > 1$. There is linear stability for $0.863 \leqslant l_1 \leqslant 1$. The minima for the three modes all occur at around $l_1 = 0.85$ to 0.87, as shown in Fig. 18.

The case of $r = 0.9$ with the other parameters identical to those of Fig. 18 results in the growth rates being roughly a reflection across the horizontal axis from those of Fig. 18. The one-fluid flow is at criticality with the outer fluid ($l_1 = 0$). There is immediate instability as l_1 leaves 0.

ACKNOWLEDGMENTS

The author wishes to thank the National Science Foundation Research Opportunities for Women Program.

This research was funded by the National Science Foundation Grant No. DMS-8615203.

[1]M. E. Charles and P. J. Redberger, Can. J. Chem. Eng. **40**, 70 (1962).
[2]D. Hasson, U. Mann, and A. Nir, Can. J. Chem. Eng. **48**, 514 (1970).
[3]A. E. Everage, Jr., Trans. Soc. Rheol. **17**, 629 (1973).
[4]J. L. White and B.-L. Lee, Trans. Soc. Rheol. **19**, 457 (1975).
[5]J. H. Southern and R. L. Ballman, Appl. Polym. Symp. **20**, 175 (1973).
[6]D. L. MacLean, Trans. Soc. Rheol. **17**, 385 (1983).
[7]N. Minagawa and J. L. White, Polym. Eng. Sci. **15**, 825 (1975).
[8]C. E. Hickox, Phys. Fluids **14**, 251 (1971).
[9]D. D. Joseph, M. Renardy, and Y. Renardy, J. Fluid Mech. **141**, 309 (1984).
[10]A. P. Hooper and W. G. C. Boyd, J. Fluid Mech. **128**, 507 (1983).
[11]Y. Renardy and D. D. Joseph, J. Fluid Mech. **150**, 381 (1985).

[12]P. T. Than, F. Rosso, and D. D. Joseph, Int. J. Eng. Sci. **40**, 70 (1987).
[13]C-S. Yih, J. Fluid Mech. **27**, 337 (1967).
[14]D. Gottlieb and S. A. Orszag, *Numerical Analysis of Spectral Methods: Theory and Applications*, CBMS–NSF Regional Conference Series in Applied Mathematics 26 (SIAM, Philadelphia, 1977).
[15]S. A. Orszag, J. Fluid Mech. **50**, 689 (1971).
[16]P. G. Drazin and W. H. Reid, *Hydrodynamic Stability* (Cambridge U.P., Cambridge, England, 1982).
[17]C.-H. Li, Phys. Fluids **12**, 2473 (1969).
[18]Y. Renardy, Phys. Fluids **28**, 3441 (1985).
[19]A. P. Hooper, Phys. Fluids **28**, 1613 (1985).
[20]Y. Renardy, Phys. Fluids **30**, 1627 (1987).